Thin-Walled Structures 64 (2013) 94–102

Contents lists available at SciVerse ScienceDirect

Thin-Walled Structures

journal homepage: www.elsevier.com/locate/tws

Buckling strength of thin-shell concrete arch dams

A. Zingoni *, K. Mudenda, V. French, B. Mokhothu

Department of Civil Engineering, University of Cape Town, Rondebosch 7701, Cape Town, South Africa

ARTICLE INFO

Article history:
Received 26 September 2011
Received in revised form
9 December 2012
Accepted 9 December 2012
Available online 12 February 2013

Keywords:
Arch dam
Shell buckling
Thin shell
Elliptic paraboloid
Cylindrical shell
Hydrostatic loading

ABSTRACT

An investigation has been undertaken on the buckling strength of concrete arch dams in the form of thin shells of single and double curvature. When subjected to the hydrostatic pressure exerted by the retained water, the shell experiences predominantly compressive internal actions, which can result in buckling failure of the thin shell. There are many factors influencing the buckling strength of the arch dam. These include the shape of the valley, the geometry of the arch surface, the degree of bulging of the arch, shell-thickness variation and support conditions. The present study makes use of FEM modelling to determine the influence of key parameters on the critical buckling pressure of cylindrical and elliptic-paraboloidal arch dams. For cylindrical arch dams, design curves giving information on factors of safety against buckling are presented. By comparing the results for the elliptic paraboloid with those for the parabolic cylindrical arch, the benefits of double curvature are evaluated.

© 2012 Elsevier Ltd. All rights reserved.

1. Introduction

The problem of the buckling of high arch dams is a complex one, owing to the large number of variables involved, such as the shape of the valley across which the dam is built, the geometry adopted for the arch (many possibilities exist), the foundation conditions at the bottom and on the sides, and so forth. Ideally, the arch should be in a state of pure membrane compression (with negligible bending moments) under full-load conditions (i.e. when the dam is full of water), to ensure the most efficient utilisation of material (materials being generally more efficient in direct tension or compression than in flexure), but there will always be some bending stresses, particularly in the vicinity of the shell boundary [1].

In searching for efficient shapes for the arch dam, the membrane method has been quite successful. This involves subjecting an initially flat membrane, oriented in the vertical plane with sides and the bottom edge clamped in a frame, to lateral water pressure, and noting the shape of the deformed membrane. Reverse hydrostatic loading on a concrete shell with the same shape should result in pure compression in the concrete, but this will not be strictly so in the vicinity of the supported edges, because the flexural rigidity of the shell will attract bending moments. To avoid the high costs of such experimental form finding, some investigators have proposed numerical procedures for the computational simulation of the membrane method [2].

There have been numerous studies on arch dams concerned with shape optimisation, strength and stability. The shape of the arch dam plays a very important role in the design of arch dams, and a lot of effort has gone into finding the most optimum shape of arch dams under given boundary constraints. In Spain, Delgado and Marquez [3] made use of polynomial curves to model the geometry of the upstream and downstream surfaces of the dam wall. In China, Li and others [4] have proposed a modified complex method to tackle the shape optimisation problem. Based on safety indexes against tensile-stress failure and elastic-buckling failure, Xie et al. [5] considered the concrete arch dam of parabolic double curvature under hydrostatic loading, and performed a shape optimisation with the strain energy of the dam being taken as the objective function. In Iran, various techniques aimed at improving conventional shape optimisation methods have been proposed [6,7].

The issue of safety of arch dams, particularly high dams, is a major consideration in design. Eigenvalue linear buckling analysis of a high arch dam has been conducted by Zhou and Chang [8], who considered the dam to be safe against buckling if the calculated buckling load was greater than the strength-limit load. Thus the idea was to ensure that when the dam failed, this would be by material failure, not buckling failure. A study for the evaluation of relevant factors of safety has recently been proposed by Jin and co-workers [9]. An improved analytical method for the calculation of stresses in arch dams has been presented by Li et al. [10], who treated the shell as an interacting system of horizontal arches and curved cantilevers in vertical planes, and imposed conditions of force equilibrium and displacement compatibility between adjacent elements.

* Corresponding author. Tel.: +27 21 650 2601; fax: +27 21 650 3293.
E-mail address: alphose.zingoni@uct.ac.za (A. Zingoni).

0263-8231/$ - see front matter © 2012 Elsevier Ltd. All rights reserved.
http://dx.doi.org/10.1016/j.tws.2012.12.001

The problem of the buckling of arch dams belongs to the more fundamental subject of the buckling of shells, a topic on which numerous studies (theoretical, experimental and numerical) have been undertaken in the past 50 years. Just to mention a few of the more recent studies, Papadakis [11] has presented an analytical solution for the buckling of thick cylindrical shells under external pressure, such a solution being applicable to the situation of certain arch dams, among other applications. The buckling of shells of revolution under hydrostatic internal pressure is, of course, a different situation to the buckling of arch dams, but studies in this area can provide useful insights on the effect of geometry on shell response. Recent studies on liquid containment shells of revolution include the work of Magnucki et al. [12] on optimum design of horizontal cylindrical tanks, the investigations of Hafeez et al. [13] and of Sweedan and El Damatty [14] on the behaviour of conical-cylindrical tanks, and the work of Zhan and Redekop [15] on the buckling and collapse behaviour of toroidal tanks. For a more detailed overview of the literature on shell buckling, the review of Teng [16] may be consulted.

2. The need for comprehensive design guidelines for arch dams

The research on arch dams that has been reported in the literature has mostly comprised case studies of actual dams constructed worldwide to date. Although important lessons can be learnt from such studies, the data upon which the observations are based is very site-specific, making it difficult to apply the results to new designs that may be required elsewhere.

It is acknowledged that attempting to generalise design situations which are generally all different from each other results in loss of design precision and the optimisation that goes with it. However, such an approach can have merit in the preliminary stages of the design process, where the objective is simply to establish which alternatives are viable, and details are not too important.

Real arch dams with irregular boundaries and non-uniform support conditions can be idealised as simpler models with straight-sided boundaries and support conditions that remain uniform over a given edge. Fig. 1 shows four examples of idealisations of the valley shape (which in turn define the boundaries of the arch). In these examples, the valley cross-section is assumed to be roughly symmetrical about a vertical axis (this is actually the case in many practical situations), which allows us to define the shape of the valley on the basis of only a small set of parameters $\{a,b,c,d\}$. If the ratios of these parameters (b/a; c/a; d/c etc) are regarded as variables, an infinite number of possibilities can be covered. The horizontal top edge of the arch dam (of length $2a$ in Fig. 1) will, of course, always be a free edge. All the other edges may be assumed to be fixed (which is practically the case in most situations).

Fig. 2 illustrates typical shell-thickness variations in the vertical section, while Fig. 3 depicts possible surface geometries of the arch dam. In Fig. 3, the retained water would be in contact with the face of the arch that is away from the centre of curvature of the shell midsurface (i.e. the water pressure acts in a direction towards the centre of curvature of the shell at any given point).

By combining the simplified valley shapes with all possible surface geometries of the arch dam (singly-curved and doubly-curved shells), and with all practical thickness variations of the concrete shell, we can assemble a comprehensive set of arch-dam options. These can then be studied individually to extract important characteristics like buckling strength and buckling modes, critical stresses for material failure in tension and compression, natural frequencies of vibration, etc. A database of basic characteristics of each type of arch dam can thus be assembled.

Given a new design situation with site-specific characteristics (such as shape of valley, dam height, geotechnical conditions) and particular design requirements with regard to safety and economy, we can use such a database to identify suitable options, and then pursue these in detail. A database of this kind does not exist, and there is a general lack of guidance of this nature in the open literature. A programme of research has been commenced at the University of Cape Town, with the objective of creating a database and providing much-needed guidance on the design of concrete arch dams. Preliminary findings on shells of single curvature have been reported at a recent conference [17]. This paper is a more comprehensive account of the results, and extends the investigation to shells of double curvature, specifically elliptic paraboloids.

3. Scope of present study

In this study, we first focus attention on arch dams of single curvature, set in a rectangular valley (Fig. 1b). We consider

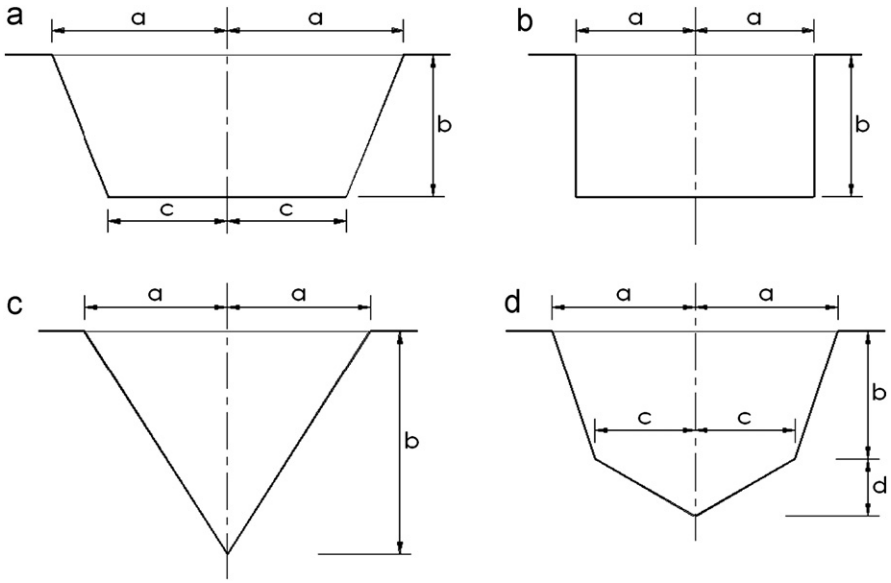

Fig. 1. Idealised shapes of dam valleys: (a) trapezoidal; (b) rectangular; (c) triangular; and (d) trapezoidal-triangular.

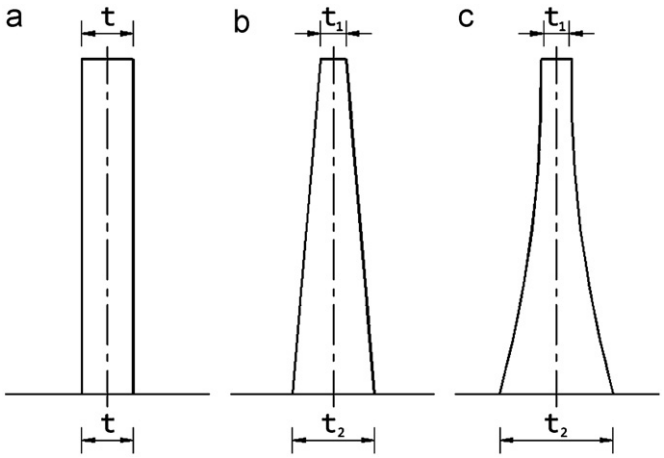

Fig. 2. Typical depthwise variations of the thickness of the concrete shell: (a) constant thickness t; (b) linear variation (from t_1 to t_2); and (c) parabolic variation (from t_1 to t_2).

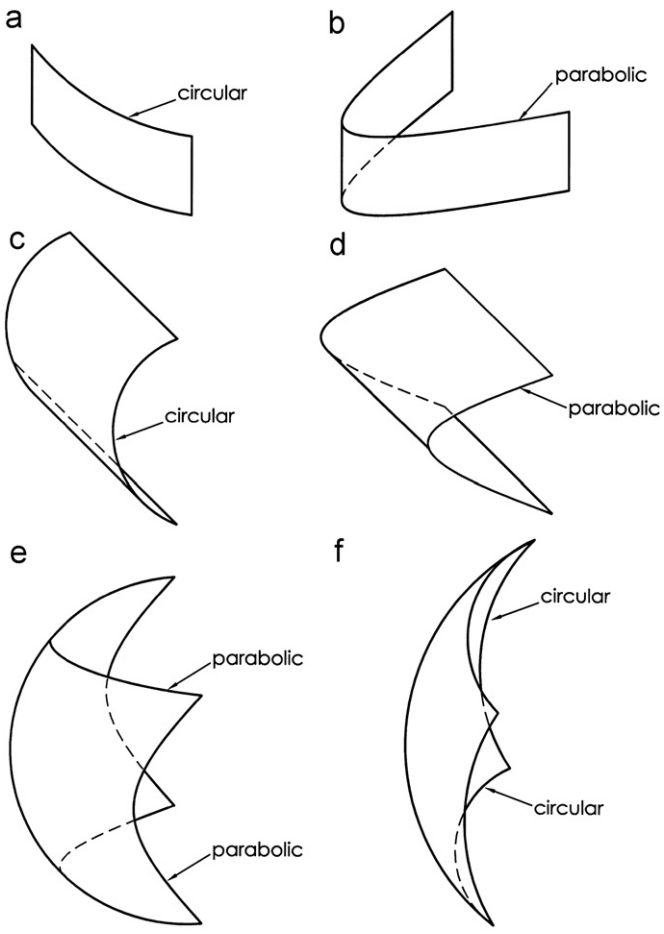

Fig. 3. Some possible mid-surface geometries of the concrete shell: (a) horizontally-curved circular cylinder; (b) horizontally-curved parabolic cylinder; (c) vertically-curved circular cylinder; (d) vertically-curved parabolic cylinder; (e) elliptic paraboloid; and (f) toroid/spheroid.

horizontally-curved arches of circular and parabolic profile (Fig. 3a and b), where the horizontal bulge of the shell relative to the vertical plane connecting the left and right abutments will be referred to as the rise h of the shell. The two cases are depicted in Fig. 4. The ratio b/a will be referred to as the aspect ratio of the dam, while the ratio h/a will be referred to as the rise ratio of the shell. The thickness of the shell is assumed to be constant in this initial study (varying wall

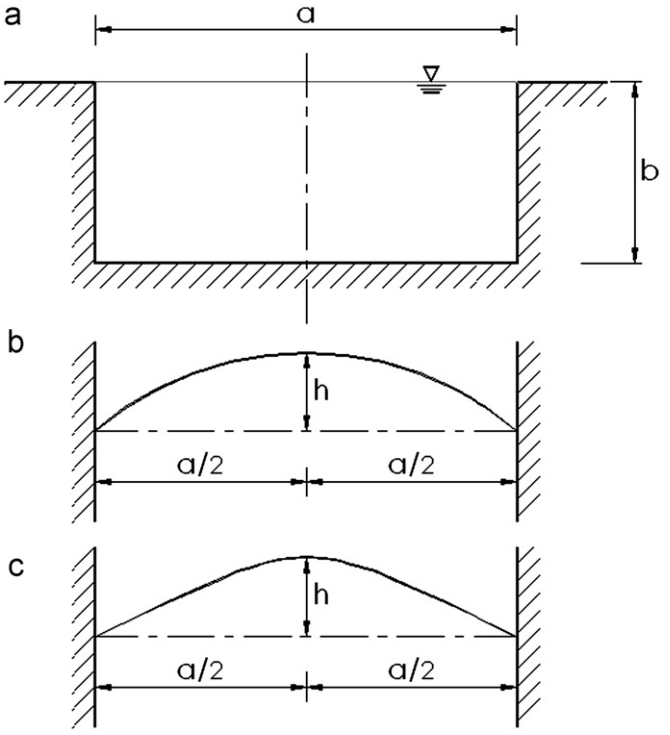

Fig. 4. Horizontally-curved arch dam in a rectangular valley: (a) front view (projection on a vertical plane); (b) plan view (circular arch); (c) plan view (parabolic arch).

thickness will be the subject of later studies), and the dam is assumed to be filled to capacity with water of unit weight 10 kN/m^3. We want to investigate the dependence of the critical buckling pressure on parameters such as a, t, h/a and b/a. Parametric studies of this type can be useful in understanding the buckling behaviour of shell panels intended for other applications [18].

The present investigation is only concerned with the behaviour of the shell up to the point when it first buckles, and post-buckling behaviour is of no interest in this context. The justification for limiting the analysis to linear elastic bifurcation is the fact that we are choosing to define failure of the arch dam, for design purposes, as the instance when first elastic buckling occurs, although it is recognised that the buckled shell would still exhibit post-buckling resistance until the point of actual collapse of the arch dam. As future work, the maximum load-carrying capacity of the buckled arch dam will be sought, and in these envisaged studies, the modelling will require to be extended into the highly nonlinear post-buckling range of shell response.

4. FEM modelling and parametric study

The following material properties were assumed for concrete:

$E = 28 \times 10^9$ N/m^2 (Young's modulus)

$\nu = 0.15$ (Poisson's ratio)

The general purpose finite element programme ABAQUS was used for the analysis. The arch was modelled with 8-node doubly curved thick quadrilateral shell elements with reduced integration. The edges were fully restrained, except along the top edge (free). A linear eigenvalue buckling analysis was then performed. A triangular variation of loading with a value of zero at the top and 1 kN at the base of the wall was used to simulate the

hydrostatic loading. The required eigenvalues (buckling loads) were then obtained as multiples of this applied loading.

The detailed numerical investigation was conducted in the form of a parametric study. With the parameter a fixed first at 50 m and then at 100 m, the aspect ratio b/a was varied from 0.25 to 2.0 in increments of 0.25, and for each aspect ratio, the critical buckling pressure (i.e. the lowest buckling load) was determined for three different values of the thickness parameter t (0.5 m, 1.0 m, 2.0 m) and three representative values of the rise ratio h/a (5%, 10%, 25%), giving a total of 144 cases. This was done for both the circular dam and the parabolic dam.

5. Numerical results

Fig. 5 shows some typical mode shapes for the circular arch. The results for the critical buckling pressures for the various cases that were analysed revealed that there is very little difference between corresponding results for the circular and parabolic profiles. Table 1 compares buckling pressures between the circular and parabolic profiles, taking the case when $t=1.0$ m and $h=10\%$. The difference between the results is less than 1% for the 50 m wide dam, and less than 1.5% for the 100 m wide dam. This was generally the case with all other combinations of parameters. Henceforth, it will suffice to consider the results for the circular cylindrical arch only (the conclusions would be equally applicable to the parabolic cylindrical arch).

The obtained results for the critical buckling pressure p_{cr} (in kN/m^2) are plotted versus the aspect ratio b/a in Figs. 6–8. These three figures relate to shell-thickness (t) values of 0.5 m, 1.0 m and 2.0 m respectively, with the upper plots pertaining to the case when $a=50$ m and the lower plots pertaining to the case when $a=100$ m. Each chart has three curves corresponding to the three rise ratios h/a of interest (5%, 10%, 25%). The dashed line coming from the

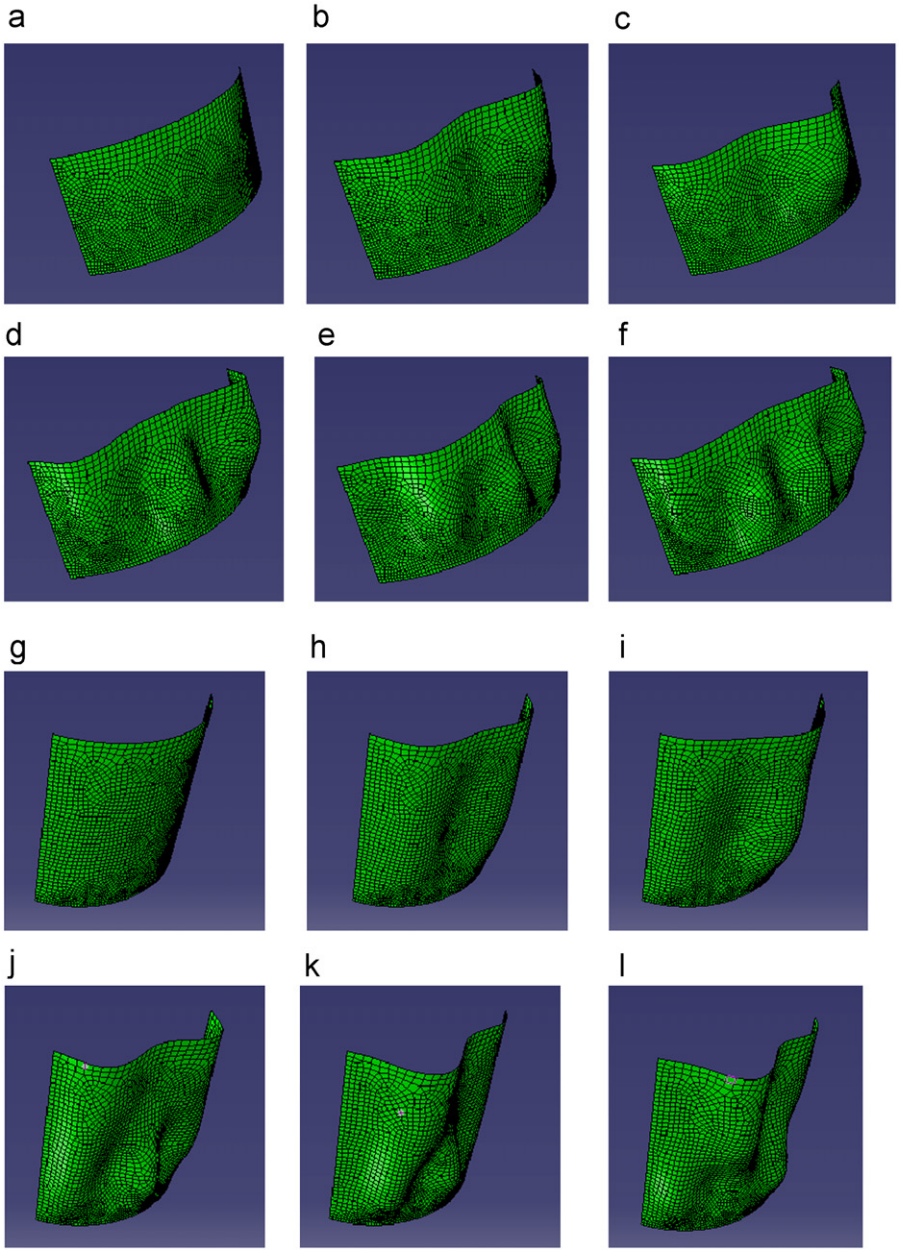

Fig. 5. Buckling modes for the circular cylindrical arch with $a=50$ m, $t=1.0$ m and $h/a=25\%$: (a) undeformed arch with $b/a=0.5$; (b)–(f) first five buckling modes for $b/a=0.5$; (g) undeformed arch with $b/a=1.0$; (h)–(l) first five buckling modes for $b/a=1.0$.

Table 1
Results of the parabolic arch versus the circular arch.

b/a	$a=50$ m; $t=1.0$ m; $h=10\%$ critical buckling pressure p_{cr} (kN/m^2)			$a=100$ m; $t=1.0$ m; $h=10\%$ critical buckling pressure p_{cr} (kN/m^2)		
	Circular	Parabolic	% Diff.	Circular	Parabolic	% Diff.
0.25	18,845.0	18,969.0	+0.66	2460.0	2490.0	+1.22
0.50	8210.0	8221.0	+0.13	1090.0	1100.0	+0.92
0.75	5177.0	5184.0	+0.14	755.0	764.0	+1.19
1.00	3992.0	4001.0	+0.23	607.0	614.0	+1.15
1.25	3381.0	3389.0	+0.24	522.0	529.0	+1.34
1.50	3000.0	3007.0	+0.23	469.0	475.0	+1.28
1.75	2735.0	2741.0	+0.22	434.0	440.0	+1.38
2.00	2538.0	2543.0	+0.20	408.0	414.0	+1.47

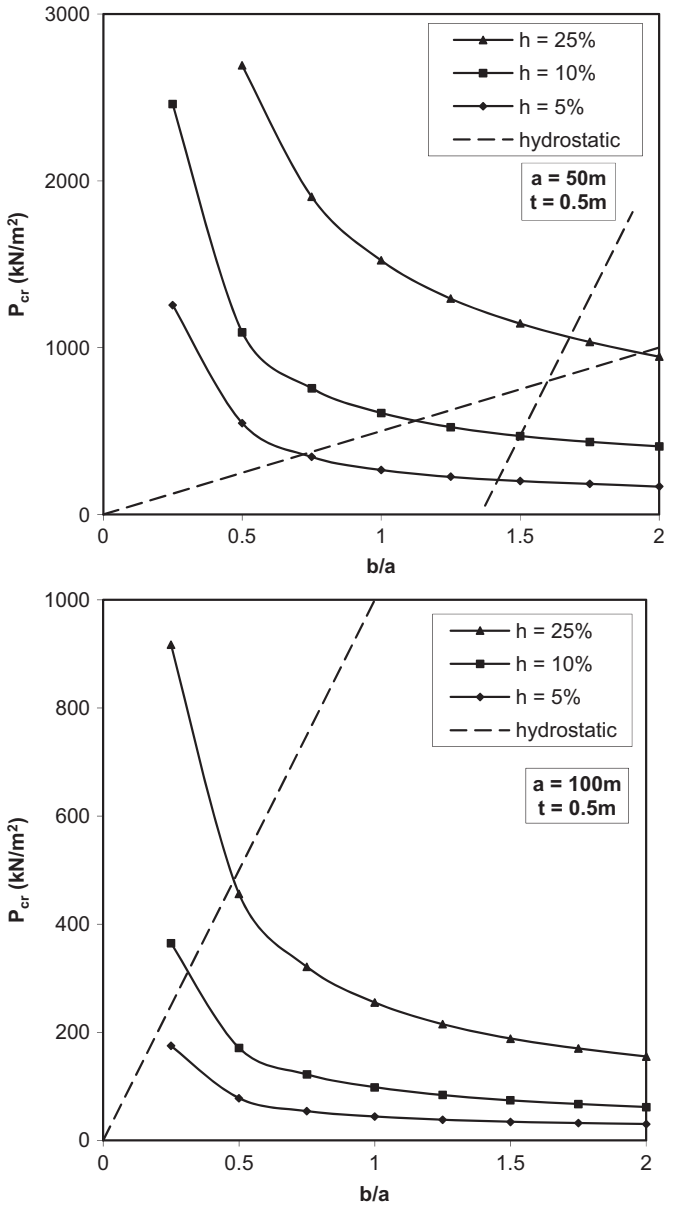

Fig. 6. Critical buckling pressure plots for the horizontally-curved circular-cylindrical arch dam of constant thickness $t=0.5$ m.

origin is the hydrostatic-pressure line (i.e. the water pressure at the base of the dam wall corresponding to the b value in question, assuming a value of 10 kN/m^3 for the unit weight of water).

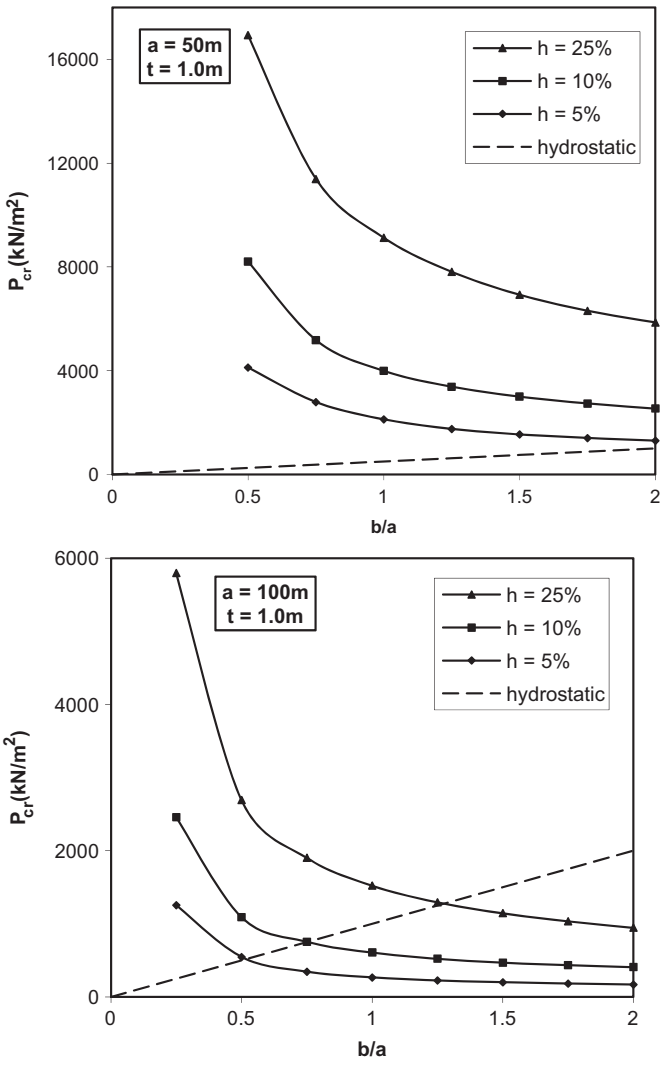

Fig. 7. Critical buckling pressure plots for the horizontally-curved circular-cylindrical arch dam of constant thickness $t=1.0$ m.

6. Discussion

From Figs. 6–8, it is clear that the buckling pressures decrease sharply with increasing relative depth (i.e. aspect ratio b/a) of the arch dam, the rate of decrease becoming slower as b/a gets larger. The shell rise ratio h/a has a strong influence on the buckling strength of the arch dam, and therefore can be used as a tool for enhancing the buckling strength of an arch of given dimensions $a \times b$ without having to increase the shell thickness, thus saving on the volume of material (concrete) used in the construction. The relative benefits of enhancing shell rise are generally greater the thinner the shell is (compare corresponding results as t is reduced from 2.0 m to 1.0 m, and from 1.0 m to 0.5 m).

As expected, the wider the arch dam becomes (i.e. the bigger the a), the lower the buckling strength becomes for the same depth of dam wall. For the same panel aspect ratio b/a, the buckling strength reduces even more rapidly as the dimension a is increased (e.g. when a is doubled from 50 m to 100 m, the buckling strength reduces to a sixth). Thus buckling strength is strongly dependent on the *scale* of the structure, for the same wall-thickness prescription. However, if the thickness t is also increased in the same proportion as a and b (e.g. if a, b and t are all doubled at the same time), then the critical buckling pressure of the shell remains the same for the same rise ratio h/a.

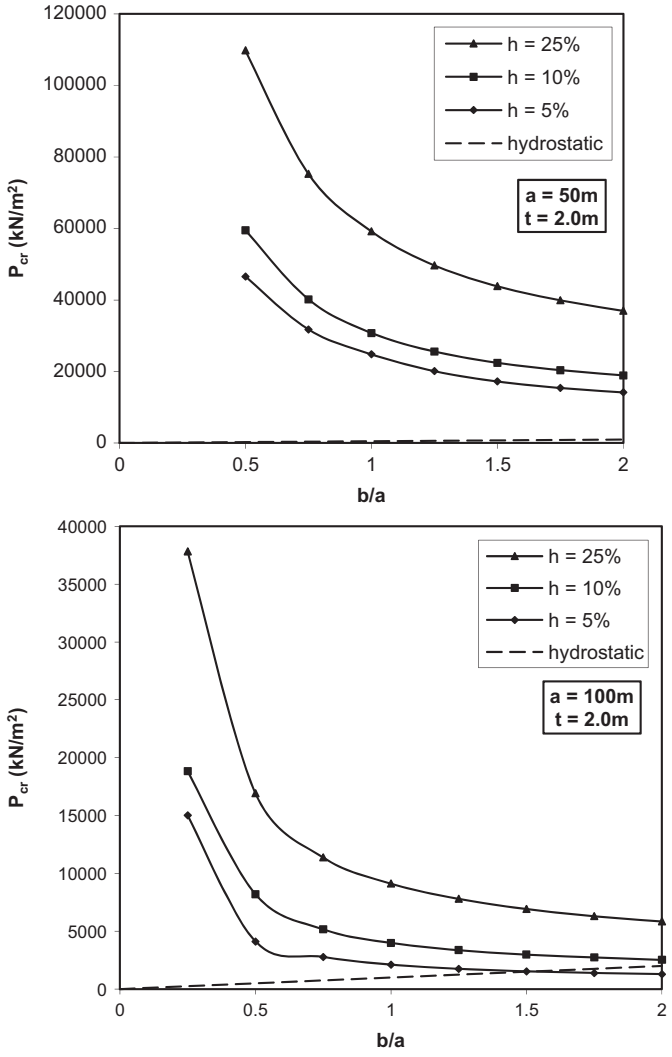

Fig. 8. Critical buckling pressure plots for the horizontally-curved circular-cylindrical arch dam of constant thickness $t=2.0$ m.

The hydrostatic pressure line in Figs. 6–8 has important design significance. If a point on the plots is above this line, it shows that the shell buckles at a pressure that is larger than the applied water pressure, so the dam will be safe. For points that fall below this line, the applied water pressure exceeds the buckling strength of the arch dam, and therefore the arch dam will experience buckling failure under the water loading.

The intersection of the hydrostatic pressure line with each curve has a particularly special significance. It gives the depth of dam wall for which the applied water pressure (when the dam is full) just causes buckling. We will call this the critical depth b_{cr}. Some values of critical depths are as follows:

For $a=50$ m, $t=0.5$ m:	$b_{cr}=36$ m for $h/a=5\%$
	$b_{cr}=56$ m for $h/a=10\%$
	$b_{cr}=97$ m for $h/a=25\%$
For $a=100$ m, $t=0.5$ m:	$b_{cr}=21$ m for $h/a=5\%$
	$b_{cr}=30$ m for $h/a=10\%$
	$b_{cr}=48$ m for $h/a=25\%$
For $a=100$ m, $t=1.0$ m:	$b_{cr}=53$ m for $h/a=5\%$
	$b_{cr}=76$ m for $h/a=10\%$
	$b_{cr}=128$ m for $h/a=25\%$

Table 2
Factors of safety against buckling for shell thickness $t=0.5$ m.

b/a	η values for $a=50$ m			η values for $a=100$ m		
	$h=5\%$	$h=10\%$	$h=25\%$	$h=5\%$	$h=10\%$	$h=25\%$
0.25	10.0	19.7	46.4	0.70	1.5	3.7
0.50	2.2	4.4	10.8	0.16	0.34	0.91
0.75	0.92	2.0	5.1	0.072	0.16	0.43
1.00	0.53	1.2	3.0	0.044	0.098	0.26
1.25	0.36	0.84	2.1	0.030	0.067	0.17
1.50	0.27	0.63	1.5	0.023	0.049	0.13
1.75	0.21	0.50	1.2	0.018	0.038	0.097
2.00	0.17	0.41	0.95	0.015	0.031	0.078

Table 3
Factors of safety against buckling for shell thickness $t=1.0$ m.

b/a	η values for $a=50$ m			η values for $a=100$ m		
	$h=5\%$	$h=10\%$	$h=25\%$	$h=5\%$	$h=10\%$	$h=25\%$
0.25	–	–	–	5.0	9.8	23.2
0.50	16.5	32.8	67.7	1.1	2.2	5.4
0.75	7.4	13.8	30.4	0.46	1.0	2.5
1.00	4.2	8.0	18.2	0.27	0.61	1.5
1.25	2.8	5.4	12.5	0.18	0.42	1.0
1.50	2.1	4.0	9.2	0.13	0.31	0.76
1.75	1.6	3.1	7.2	0.10	0.25	0.59
2.00	1.3	2.5	5.9	0.085	0.20	0.47

Table 4
Factors of safety against buckling for shell thickness $t=2.0$ m.

b/a	η values for $a=50$ m			η values for $a=100$ m		
	$h=5\%$	$h=10\%$	$h=25\%$	$h=5\%$	$h=10\%$	$h=25\%$
0.25	–	–	–	60.1	75.4	151.3
0.50	186.3	238.1	439.2	8.2	16.4	33.9
0.75	84.6	107.1	200.7	3.7	6.9	15.2
1.00	49.6	61.5	118.4	2.1	4.0	9.1
1.25	32.2	40.9	79.4	1.4	2.7	6.2
1.50	22.9	29.9	58.5	1.0	2.0	4.6
1.75	17.6	23.3	45.6	0.80	1.6	3.6
2.00	14.1	18.9	37.0	0.65	1.3	2.9

If the dam depth b equals the critical depth b_{cr}, the factor of safety against buckling failure is equal to 1.0. The factor of safety against buckling failure will be defined as the ratio of the buckling strength of the concrete arch (p_{cr}) to the applied hydrostatic water pressure (p_{water}):

$$\eta = \frac{p_{cr}}{p_{water}} \tag{1}$$

An η value above 1.0 denotes a safe design, while an η value below 1.0 denotes an unsafe design. The derived plots will enable the designer to determine, via Eq. (1), exactly how safe a particular combination of design parameters is, or alternatively, to choose a set of design parameters that delivers a required factor of safety. To help in this regard, Tables 2–4 summarise the factors of safety for all the combinations of parameters studied. As expected, the factors of safety increase with increasing shell rise, and decrease with increasing depth of the dam.

7. Effect of double curvature: the elliptic paraboloid

To study the effect of doubly curving the shell (that is, in both the vertical and the horizontal directions), we consider an elliptic

Table 5
Critical buckling pressures for the elliptic paraboloid (EP) versus the parabolic cylinder (PC).

b/a	$a=50$ m; $h/a=10\%$; $t=0.5$ m critical buckling pressure p_{cr} (kN/m^2)			$a=50$ m; $h/a=10\%$; $t=1.0$ m critical buckling pressure p_{cr} (kN/m^2)			$a=50$m; $h/a=10\%$; $t=2.0$m critical buckling pressure p_{cr} (kN/m^2)		
	EP	PC	ξ	EP	PC	ξ	EP	PC	ξ
0.25	4647.0	2463.0	1.89	26,113.0	18,919.0	1.38	255,282.0	213,528.0	1.20
0.50	3609.0	1100.0	3.28	19,658.0	8200.0	2.40	98,067.0	59,525.0	1.65
0.75	3326.0	750.0	4.43	16,514.0	5175.0	3.19	85,686.0	40,163.0	2.13
1.00	2372.0	600.0	3.95	11,779.0	4000.0	2.94	64,899.0	30,750.0	2.11
1.25	1755.0	525.0	3.34	8923.0	3375.0	2.64	48,538.0	25,563.0	1.90
1.50	1365.0	473.0	2.89	6927.0	3000.0	2.31	38,675.0	22,425.0	1.72
1.75	1114.0	438.0	2.55	5752.0	2713.0	2.12	32,364.0	20,388.0	1.59
2.00	945.0	410.0	2.30	4953.0	2500.0	1.98	28,081.0	18,900.0	1.49

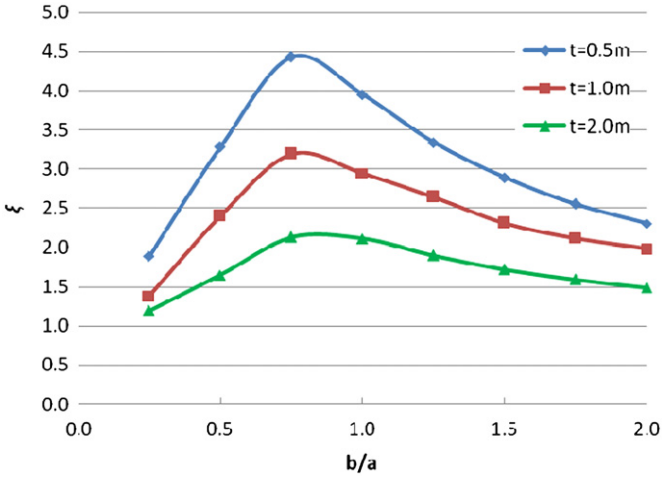

Fig. 9. Variation of ξ (ratio of critical buckling pressure for elliptic paraboloid to critical buckling pressure for parabolic cylinder) with b/a for various shell thicknesses.

paraboloid of the same aspect ratio b/a and same rise ratio h/a as the parabolic cylinder, and compare the results. The comparisons are based on a fixed width of the arch of $a=50$ m, and a fixed rise ratio of $h/a=10\%$.

In Table 5, the critical buckling pressures for such an elliptic paraboloid are shown against their cylindrical-shell counterparts, for three values of shell thickness ($t=0.5$ m; $t=1.0$ m; $t=2.0$ m), and b/a ratios of the arch ranging from 0.25 to 2.00 as before. The parameter ξ denotes the factor by which the critical buckling pressure of the parabolic cylinder is enhanced by giving it the double curvature of the elliptic paraboloid while maintaining the same aspect ratio and same rise ratio. It is the ratio of the critical buckling pressures for the elliptic paraboloid to that of the corresponding parabolic cylinder. The variation of ξ with b/a for the three values of shell thickness is shown in Fig. 9.

We observe from Fig. 9 that the beneficial effect of double curvature becomes higher as the shell becomes thinner. Also, this beneficial effect (as measured by the value of the parameter ξ) increases as the aspect ratio is increased from the starting value of 0.25 (that is, as the depth of the arch is increased), until it peaks at an aspect ratio of $b/a=0.75$ for the thinner shells ($t=0.5$ m; $t=1.0$ m) and $b/a=0.83$ for the thicker shell ($t=2.0$ m). The peak values of ξ are 4.4, 3.2 and 2.3 for $t=0.5$ m, $t=1.0$ m and $t=2.0$ m respectively. Beyond these values of b/a, the beneficial effect of double curvature progressively decreases, with ξ eventually reaching values of 2.3 (for $t=0.5$ m), 2.0 (for $t=1.0$ m) and 1.5 (for $t=2.0$ m) at the maximum aspect ratio of 2.0 covered by this study. Even for such relatively narrow and deep dams, the effect of double curvature still remains significant and worth exploiting.

Fig. 10 depicts the first buckling mode of the elliptic paraboloid under hydrostatic pressure, for various combinations of aspect ratio b/a and shell thickness t. It is clear that the buckling patterns of the shell are very much dependent on these two parameters. Shallow walls show more buckling displacement near the top edge (which is free), and the zones of maximum displacement migrate downwards as the depth of the wall is increased. However, because of the restraint at the bottom, this downward migration eventually stops. The buckling-displacement variation across the dam width is also more rapid the thinner the shell is.

8. Summary and conclusions

In this study, we have investigated the buckling behaviour of vertical concrete arch dams which are curved in plan, as part of a wider programme of research aimed at generating a database of design characteristics for a wide range of arch-dam types. The results have been presented in the form of user-friendly design charts, which allow a safe combination of design parameters to be chosen, at the same time providing an indication of the factor of safety associated with an adopted design.

A number of significant observations have been made. First, the actual mathematical shape of the arch (circular or parabolic) does not have a significant effect on the buckling strength. Other geometric properties (such as shell thickness t, rise ratio h/a and aspect ratio b/a) have a far greater effect. The buckling pressures are seen to decrease sharply with increasing relative depth (i.e. aspect ratio) of the arch dam, the rate of decrease becoming slower as b/a gets larger. The shell rise ratio has a particularly strong influence on the buckling strength of the arch dam, and therefore can be used as a tool for enhancing the buckling strength of an arch of given dimensions $a \times b$ without having to increase the shell thickness, thus saving on the volume of material (concrete) used in the construction.

It must be pointed out that the question of whether it is material strength or buckling capacity that governs the design of the concrete arch has not been addressed in this paper. It is possible that some of the obtained values of critical buckling pressures are associated with stress levels that are well above material strengths in tension and compression, implying that failure of the material would occur first before the shell buckles. In particular, the highly restrained conditions at the bottom and lower sides of the shell, combined with large values of the hydrostatic pressure prevailing in these locations, are expected to induce in the shell relatively large bending effects of a fluctuating but rapidly decaying character, similar to that observed for containment shells of revolution [19–23]. These effects could lead to cracking and material failure of the concrete before the onset of buckling. The purpose of the present study was to establish buckling strengths and factors of safety against buckling, but clearly the issue of other possible ways of failing would also need to be considered in the course of a full design.

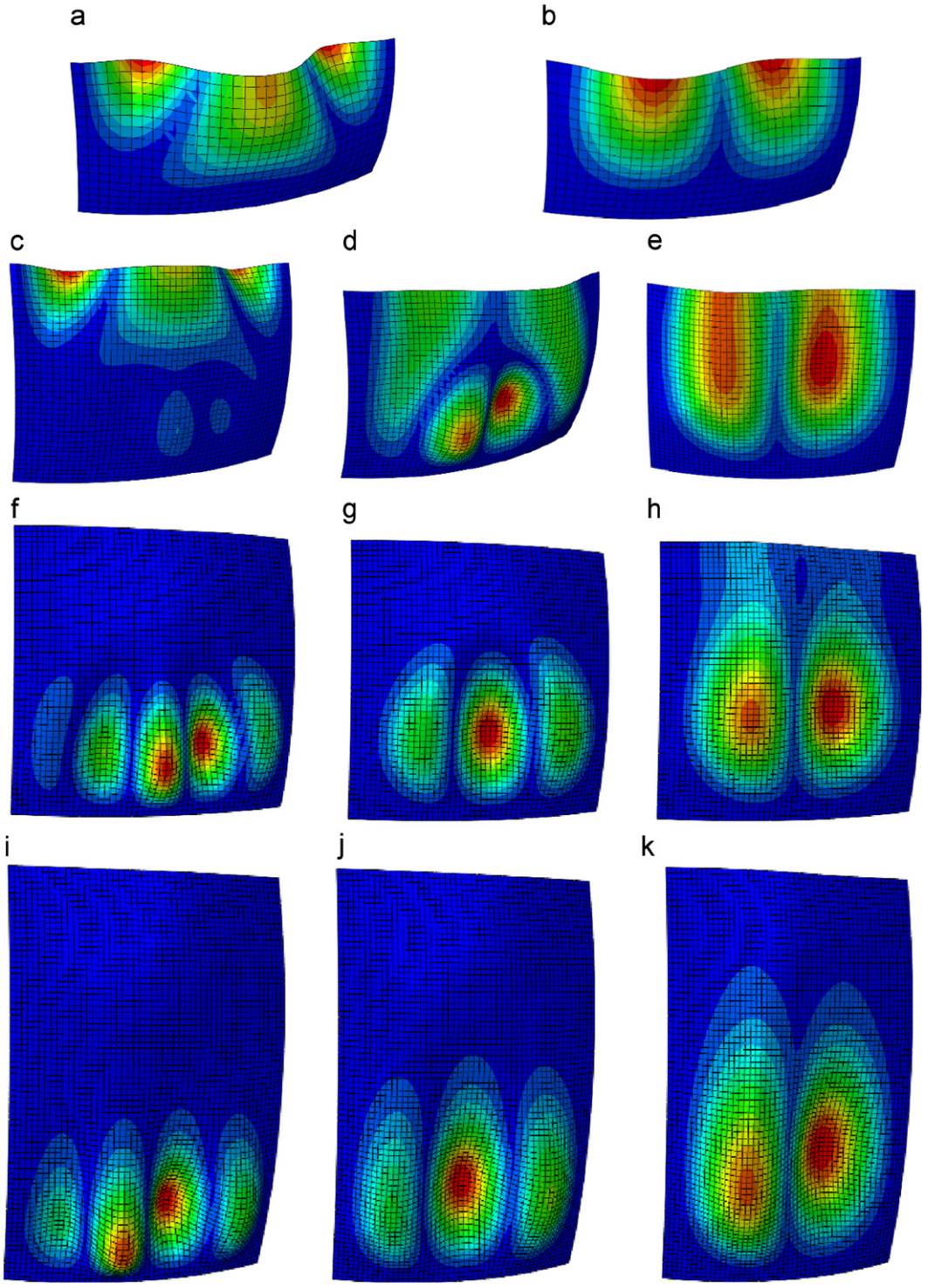

Fig. 10. First buckling modes for the elliptic paraboloid: (a) $b/a=0.50$; $t=1.0$ m; (b) $b/a=0.50$; $t=2.0$ m; (c) $b/a=0.75$; $t=0.5$ m; (d) $b/a=0.75$; $t=1.0$ m; (e) $b/a=0.75$; $t=2.0$ m; (f) $b/a=1.00$; $t=0.5$ m; (g) $b/a=1.00$; $t=1.0$ m; (h) $b/a=1.00$; $t=2.0$ m; (i) $b/a=1.50$; $t=0.5$ m; (j) $b/a=1.50$; $t=1.0$ m; (k) $b/a=1.50$; $t=2.0$ m.

The beneficial effect of double curvature has also been quantified. Depending on the thickness of the shell wall, this maximises in the aspect-ratio range $0.7 \leq b/a \leq 0.9$. For the parametric ranges covered in this study, the critical buckling pressure for the elliptic paraboloid has been found to be typically 2 to 5 times higher than that of the corresponding parabolic cylinder, the higher values of ξ being associated with the thinner range of shells.

Ongoing studies are considering more complicated valley shapes, arch dams in the form of shells of other double-curvature configurations (elliptic hyperboloids and toroidal surfaces), walls of varying thickness (linear and parabolic), effect of vertical rib stiffeners, nonlinear material behaviour, and postbuckling response of the shell arch.

References

[1] Zingoni A. Shell structures in civil and mechanical engineering. London: Thomas Telford Publishing; 1997.

[2] Da Silva VD, Julio ENBS. Computation of membrane shapes and analysis of arch dams. Computers and Structures 1997;64(1–4):849–55.
[3] Delgado AH, Marquez L. Modelling of an arch dam by polynomial interpolation. Mathematics and Computers in Simulation 2009;79:3434–43.
[4] Li S, Ding L, Zhao L, Zhou W. Optimization design of arch dam shape with modified complex method. Advances in Engineering Software 2009;40:804–8.
[5] Xie NG, Sun LS, Zhao L, Fang H. Dam shape's optimization design based on strain energy. Journal of Hydraulic Engineering 2006;37(11):1342–7.
[6] Akbari J, Ahmadi MT, Moharrami H. Advances in concrete arch dams shape optimization. Applied Mathematical Modelling 2011;35:3316–33.
[7] Hamidian D, Seyedpoor SM. Shape optimal design of arch dams using an adaptive neuro-fuzzy inference system and improved particle swarm optimization. Applied Mathematical Modelling 2010;34:1574–85.
[8] Zhou W, Chang X. Stability study based on buckling analysis of high arch dam. In: Proceedings of the international symposium on safety science and technology. Part A; 2004. 477–82.
[9] Jin F, Hu W, Pan J, Yang J, Wang J, Zhang C. Comparative study procedure for the safety evaluation of high arch dams. Computers and Geotechnics 2011;38:306–17.
[10] Li S, Chen Y, Li J, Yang J. The new method of arch dam stress calculation and the application of GTSTRUDL CAE/CAD system. Advances in Engineering Software 2000;31:303–7.
[11] Papadakis G. Buckling of thick cylindrical shells under external pressure: a new analytical expression for the critical load and comparison with elasticity solutions. International Journal of Solids and Structures 2008;45:5308–21.
[12] Magnucki K, Lewinski J, Stasiewicz P. Optimal sizes of a ground-based horizontal cylindrical tank under strength and stability constraints. International Journal of Pressure Vessels and Piping 2004;81:913–7.
[13] Hafeez G, El Ansary AM, El Damatty AA. Stability of combined imperfect conical tanks under hydrostatic loading. Journal of Constructional Steel Research 2010;66:1387–97.
[14] Sweedan AMI, El Damatty AA. Simplified procedure for design of liquid-storage combined conical tanks. Thin-Walled Structures 2009;47:750–9.
[15] Zhan HJ, Redekop D. Vibration, buckling and collapse of ovaloid toroidal tanks. Thin-Walled Structures 2008;46:380–9.
[16] Teng JG. Buckling of thin shells: recent advances and trends. Applied Mechanics Reviews, Transactions of the ASME 1996;49:263–74.
[17] Zingoni A, Mudenda K, French V. Buckling strength of concrete arch dams of single curvature. In: Proceedings of the twelfth international conference on civil, structural and environmental engineering computing, Funchal (Portugal). Paper no. 226; 2009.
[18] Zingoni A, Balden V. On the buckling strength of stiffened elliptic paraboloidal steel panels. Thin-Walled Structures 2009;47(6/7):661–7.
[19] Zingoni A. Stresses and deformations in egg-shaped sludge digesters: membrane effects. Engineering Structures 2001;23(11):1365–72.
[20] Zingoni A. Stresses and deformations in egg-shaped sludge digesters: discontinuity effects. Engineering Structures 2001;23(11):1373–82.
[21] Zingoni A. Discontinuity effects at cone-cone axisymmetric shell junctions. Thin-Walled Structures 2002;40(10):877–91.
[22] Zingoni A. Parametric stress distribution in shell-of-revolution sludge digesters of parabolic ogival form. Thin-Walled Structures 2002;40(7/8):691–702.
[23] Zingoni A. Simplification of the derivation of influence coefficients for symmetric frusta of shells of revolution. Thin-Walled Structures 2009;47:912–8.